Neutron diffraction by magnetic crystals: V_2O_3

2002 J. Phys.: Condens. Matter 14 10281

(http://iopscience.iop.org/0953-8984/14/43/324)

INSTITUTE OF PHYSICS PUBLISHING JOURNAL OF PHYSICS: CONDENSED MATTER

J. Phys.: Condens. Matter **14** (2002) 10281–10293 PII: S0953-8984(02)52187-1

Neutron diffraction by magnetic crystals: V_2O_3

E Balcar[1] **and S W Lovesey**[2]

[1] TU Vienna, Atominstitut, Stadionallee 2, A-1020 Vienna, Austria
[2] Rutherford Appleton Laboratory, Chilton, Oxfordshire OX11 0QX, UK

Received 9 August 2002
Published 18 October 2002
Online at stacks.iop.org/JPhysCM/14/10281

Abstract

A theory of neutron scattering by magnetic ions is developed and applied to diffraction by crystals in which ions in the unit cell are not equivalent on account of a lack of translational symmetry in their environments. The development demonstrates a close connection between interpretations of magnetic neutron and x-ray Bragg diffraction, in terms of an atomic model. Cross-sections for neutron diffraction by powders and single crystals, including polarization-induced interference between nuclear and magnetic amplitudes, are considered. By way of illustrating the theoretical development, cross-sections are predicted for Mott–Hubbard insulator, V_2O_3, on the basis of findings from extensive studies using resonant x-ray diffraction.

1. Introduction

The determination of magnetization distributions by the Bragg diffraction of neutrons is not a new experimental technique but one that has developed over the past four decades [1]. It is a technique of paramount value in understanding modern magnetic materials whose complex properties can involve an interplay of charge, orbital and spin degrees of freedom of the valence electrons [2, 3]. A theoretical framework for the interpretation of neutron diffraction data has also been in place for some time, starting essentially with Trammell's work [4]. Resonant and non-resonant Bragg diffraction of x-rays has come to the fore as a complementary technique in the past decade [5] with the growing availability of intense, polarized and tunable beams of x-rays from synchrotron sources. The instrumentation now available at synchrotron sources provides accurate and detailed information on charge and magnetization distributions. As an example of recent applications of resonant x-ray diffraction revealing new features of complex magnetic materials, we will consider the Mott–Hubbard insulator V_2O_3 [6].

We calculate the intensity of neutrons diffracted from crystals that support long-range magnetic order. Ions in a unit cell are not equivalent due to a lack of translational symmetry in their environments. The present work is based on atomic models which have proved to be good starting points for the interpretation of a wealth of data on 3d transition and lanthanide compounds. A theory of neutron diffraction, with full account of scattering by spin and orbital

magnetic moments, is developed from previous work [7, 8] and applied to powder and single-crystal samples. One aim in the development is to expose common structure in frameworks for the interpretation of neutron diffraction and x-ray diffraction data. In the case of V_2O_3, neutron diffraction, at reflections revealed so far only in resonant x-ray diffraction, can make a pivotal contribution to understanding its complex magnetic properties.

Vanadium sesquioxide exhibits a first-order, ferroelastic structural phase transition, at a temperature in the range 150–160 K, at which the material changes from a metal to an insulator and from a paramagnet to a collinear antiferromagnet. The long-range magnetic order coexists with a monoclinic crystal structure with space group $I2/a$ (number 15) in which vanadium ions occupy sites 8(f) that possess no symmetry. The energy dependences of resonant x-ray scattering from V_2O_3 [6] at space-group-forbidden reflections (Miller indices hkl satisfy $h+k+l$ an odd integer) are strikingly different at reflections with even and odd values of h, and this feature has been shown to be due to a selection rule [9] that stems from the configuration of the V moments. The same theory [9] accounts for data collected in azimuthal-angle scans at space-group-forbidden reflections.

Expressions for the amplitude and intensity of magnetic neutron diffraction are recorded in the next section, where they are developed for the standard atomic model of a magnetic material. We include a new expression for the intensity which highlights contributions made to scattering by anisotropic components of the magnetization. Properties of the amplitude set in principal axes are given in section 3. Neutron diffraction by V_2O_3 is the subject of section 4, where we give an expression for the intensity expected from a single crystal. Use of the expression for the interpretation of experimental data should yield valuable information that can be compared directly with findings from *ab initio* calculations and results derived from complementary experiments. To illustrate the information content of the neutron intensity we evaluate our expression for a model V wavefunction, and our findings suggest that intensities at some matching reflections have the potential to yield good quality information about the orbital magnetization. We also estimate the intensity of reflections first seen in resonant x-ray diffraction [6]. A brief discussion of our main results appears in section 5, and material on the atomic spherical tensors at the heart of our theoretical framework is gathered in an appendix.

2. Basics

The interaction between a neutron with spin $\boldsymbol{s}_n$ and electrons with position, spin and momentum variables $\boldsymbol{R}_j$, $\boldsymbol{s}_j$ and $\boldsymbol{p}_j$, respectively, is $\boldsymbol{s}_n \cdot \boldsymbol{Q}_\perp$ where

$$\boldsymbol{Q}_\perp = \sum_j \exp(\mathrm{i}\boldsymbol{k}\cdot\boldsymbol{R}_j)\left\{\hat{\boldsymbol{k}}\times(\boldsymbol{s}_j\times\hat{\boldsymbol{k}}) - \frac{\mathrm{i}}{\hbar k^2}(\boldsymbol{k}\times\boldsymbol{p}_j)\right\}. \tag{2.1}$$

Here, $\boldsymbol{k}$ is the change on scattering in the wavevector of the neutron and $\hat{\boldsymbol{k}} = \boldsymbol{k}/k$. In an atomic model of a magnetic material the sum on j over electrons is partitioned into a sum over electrons in the valence shell of an ion and a sum over all ions. The magnetic amplitude observed in Bragg diffraction is the mean value of $\boldsymbol{Q}_\perp$, denoted here by $\langle\boldsymbol{Q}_\perp\rangle$, evaluated for magnetic ions in the unit cell. It has been shown that the magnetic amplitude can be written as

$$\langle\boldsymbol{Q}_{\perp,p}\rangle = (4\pi)^{1/2}\sum_{KK'}\sum_{qq'} Y_q^K(\hat{\boldsymbol{k}})\Psi_{q'}^{K'}(K)(KqK'q'|1p). \tag{2.2}$$

In this expression the Clebsch–Gordan coefficient couples two spherical tensors, of rank K and K', to form a tensor of rank one (a vector) and projection $p = 0, \pm 1$. The coefficient is zero unless K is equal to $|K'-1|$, K' or $K'+1$, and $p = q + q'$. Evidently, the geometric

content of the magnetic amplitude is contained in spherical harmonics $Y_q^K(\hat{\boldsymbol{k}})$. The quantity $\Psi_{q'}^{K'}(K)$ is the unit-cell structure factor:

$$\Psi_{q'}^{K'}(K) = \sum_{\boldsymbol{d}} \exp(\mathrm{i}\boldsymbol{k}\cdot\boldsymbol{d})\langle T_{q'}^{K'}(K)\rangle_{\boldsymbol{d}}, \tag{2.3}$$

where $\langle T_{q'}^{K'}(K)\rangle_{\boldsymbol{d}}$ describes the valence shell of the ion at position $\boldsymbol{d}$ in the cell. With a small value of k the atomic tensor $\langle \boldsymbol{T}^1\rangle$ is proportional to the magnetic moment $\boldsymbol{\mu} = \langle \boldsymbol{L} + 2\boldsymbol{S}\rangle$. Additional properties of atomic spherical tensors for neutron diffraction are gathered in an appendix.

The interpretation of resonant x-ray diffraction, based on an atomic model, contains a quantity very similar to (2.2) [10]. The amplitude in this instance is a scalar, i.e. a tensor of rank zero. Introducing the identity $(KqK'q'|00) \propto \delta_{K,K'}\delta_{q,-q'}$ in (2.2), the quantity which in x-ray diffraction corresponds to (2.2) is actually a scalar product of a geometric factor with the structure factor, where the geometric factor contains information on the condition of the primary and diffracted x-ray beams.

Thomson scattering of x-rays can also be expressed in terms of our unit-cell structure factor. In this case, the atomic tensor in (2.3) describes charge scattering. Appropriate expressions are (A.10) and (A.11).

Returning to neutron diffraction, we recount the limiting value taken by the magnetic amplitude as $\boldsymbol{k}$ tends to the forward direction. With $k \to 0$ one finds $\langle \boldsymbol{T}^1\rangle \to \boldsymbol{\mu}/3$ and, for one ion,

$$\langle \boldsymbol{Q}_\perp\rangle \to \tfrac{1}{2}\{\boldsymbol{\mu} - \hat{\boldsymbol{k}}(\hat{\boldsymbol{k}}\cdot\boldsymbol{\mu})\}. \tag{2.4}$$

Retaining the first correction to these limiting values leads to the so-called dipole approximation for $\langle \boldsymbol{T}^1\rangle$ in which

$$\langle \boldsymbol{T}^1\rangle \sim \tfrac{1}{3}\{2\langle \boldsymbol{S}\rangle\langle j_0(k)\rangle + \langle \boldsymbol{L}\rangle(\langle j_0(k)\rangle + \langle j_2(k)\rangle)\}. \tag{2.5}$$

In this expression, $\langle j_n(k)\rangle$ is the Bessel function transform of order n of the radial component of the magnetization distribution. The components have the properties $\langle j_0(0)\rangle = 1$ and for $n > 0\langle j_n(0)\rangle = 0$. For the interpretation of data gathered with a view to examining spatial anisotropy in the magnetization distribution, higher-order $K' > 1$ atomic tensors are considered. The upper limit is set by the angular momentum of the valence shell; for a 3d transition ion the maximum value of K' in (2.2) is 5, and for a lanthanide ion the corresponding value is 7.

The intensity observed in a powder pattern is interpreted in terms of

$$I_{\text{powder}} = \frac{1}{4\pi}\int \mathrm{d}\hat{\boldsymbol{k}}\,|\langle \boldsymbol{Q}_\perp\rangle|^2 = \sum_{KK'}\sum_{q'}\left(\frac{3}{2K'+1}\right)|\Psi_{q'}^{K'}(K)|^2. \tag{2.6}$$

This expression can be simplified by using a general property of the atomic tensor. If K' is an odd integer, then $K = K' \pm 1$, and

$$\langle T_{q'}^{K'}(K'+1)\rangle = \left(\frac{K'}{K'+1}\right)^{1/2}\langle T_{q'}^{K'}(K'-1)\rangle. \tag{2.7}$$

If K' is even, the only non-zero tensor occurs when $K = K'$.

Physical properties of the sample can impose restrictions on K' and usually one finds that K' is restricted to odd integers. There are two sources of restrictions. First, a property of states used to describe the valence shell can impose restrictions on K'. For example, if a 4f shell is adequately described by states with the same values of J, S and L, then K' is odd, for atomic tensors with even K' are zero. Secondly, the configuration of magnetic moments can

lead to a selection rule on K' in the structure factor. Such a case is V_2O_3, which is a collinear antiferromagnet, and $\Psi^{K'}$ vanishes unless K' is odd.

Experiments on single crystals are interpreted in terms of $|\langle \boldsymbol{Q}_\perp \rangle|^2$. When K' is odd the single-crystal intensity can be written in a simple and appealing form, which has the geometric content expressed in terms of spherical harmonics $Y^l_m(\hat{\boldsymbol{k}})$ instead of products of spherical harmonics. We find, from (2.2),

$$I_{\rm crystal} = |\langle \boldsymbol{Q}_\perp \rangle|^2 = (4\pi)^{1/2} \sum_{K'I'} \sum_{q'r'} \sum_{lm} Y^l_m(\hat{\boldsymbol{k}}) G(K', I'; l) \times (-1)^{r'} \Psi^{K'}_{q'}(K'-1) \{\Psi^{I'}_{r'}(I'-1)\}^* \begin{pmatrix} K' & I' & l \\ q' & r' & m \end{pmatrix}. \tag{2.8}$$

Values of $G(K', I'; l)$ are listed in table 1, and satisfy the sum rule

$$\sum_l (2l+1)^{1/2} \begin{pmatrix} K' & I' & l \\ 0 & 0 & 0 \end{pmatrix} G(K', I'; l) = 0. \tag{2.9}$$

$3j$-symbols in (2.8) and (2.9) are more convenient to use than Clebsch–Gordan coefficients;

$$\begin{pmatrix} K & I & l \\ q & r & m \end{pmatrix} = (-1)^{K-I-m} (2l+1)^{-1/2} (Kq\, Ir | l-m). \tag{2.10}$$

The quantity summed in (2.9) is also included in table 1. To demonstrate that the expression for the single-crystal intensity is purely real, one uses $G(K', I'; l) = G(I', K'; l)$ and $(Y^l_m)^* = (-1)^m Y^l_{-m}$ together with an identity for interchanging two columns of a $3j$ symbol. The term in (2.8) with $l = m = 0$ is identical to the powder intensity derived from (2.6), because integration over the direction of $\boldsymbol{k}$ sets equal to zero every term in (2.8) except the term with $l = m = 0$. Terms in (2.8) with $l > 0$ represent the influence on scattering of anisotropy in the magnetization distribution.

A useful approximation to the intensity is obtained from the term in (2.8) with $K' = I' = 1$. The corresponding value of the structure factor $\Psi^1_{q'}(0)$ is a spherical component of a vector $\boldsymbol{\Psi}^1$ with real Cartesian components. Setting $K' = I' = 1$ in (2.8), it reduces to

$$I_{\rm crystal} = \tfrac{9}{4} \{\boldsymbol{\Psi}^1 \cdot \boldsymbol{\Psi}^1 - (\hat{\boldsymbol{k}} \cdot \boldsymbol{\Psi}^1)^2\}. \tag{2.11}$$

The dipole approximation for the intensity is obtained from (2.11) on using in $\Psi^1_{q'}(0)$ the appropriate approximation for the atomic tensor.

To interpret the interference between magnetic and nuclear amplitudes induced by polarization $\boldsymbol{P}$ in the primary beam, one needs to evaluate

$$\boldsymbol{P} \cdot \langle \boldsymbol{Q}_\perp \rangle = \sum_{q=0,\pm 1} (-1)^q P_{-q} \langle Q_{\perp,q} \rangle. \tag{2.12}$$

The identity expresses the scalar product of $\boldsymbol{P}$ and $\langle \boldsymbol{Q}_\perp \rangle$ in terms of their spherical components. The Cartesian components of $\boldsymbol{P}$, say, are

$$P_x = (P_{-1} - P_{+1})/\sqrt{2}, \qquad P_y = {\rm i}(P_{-1} + P_{+1})/\sqrt{2}, \qquad P_z = P_0. \tag{2.13}$$

3. Principal axes

In many cases the physical properties of an ion in a crystal are most conveniently addressed in a set of axes that are not the crystal axes, nor the axes used to define the geometry of the experiment. Let us label the second set of axes by Cartesian coordinates $(\xi\eta\zeta)$. We use Euler angles α, β and γ to define the second set of axes, used for calculations of atomic quantities, relative to the chosen crystal axes and find

$$\langle T^K_q \rangle = \sum_r \langle T^K_r \rangle_{(\xi\eta\zeta)} D^K_{rq}(-\gamma, -\beta, -\alpha), \tag{3.1}$$

where D^K_{rq} is an element of the rotation matrix.

Table 1. Values of $G(K', I'; l)$ that appear in equation (2.8). The right-hand column is the combination of G and a $3j$-symbol $(3j)$ that arises in (2.9) and subsequent applications. Table 1(a) contains those entries relevant for 3d transition elements and table 1(b) gives the additional values required for lanthanide elements.

(a)					(b)				
K'	I'	l	$G(K', I'; l)$	$(2l+1)^{1/2}(3j)G$	K'	I'	l	$G(K', I'; l)$	$(2l+1)^{1/2}(3j)G$
1	1	0	$-\frac{3}{2}\sqrt{3}$	$\frac{3}{2}$	1	7	6	$-\frac{3}{2}\sqrt{3}$	$\frac{3}{2}\sqrt{\frac{7}{5}}$
1	1	2	$-\frac{3}{2}\sqrt{\frac{3}{2}}$	$-\frac{3}{2}$	1	7	8	$-\frac{3}{4}\sqrt{\frac{21}{2}}$	$-\frac{3}{2}\sqrt{\frac{7}{5}}$
1	3	2	$-\frac{3}{2}\sqrt{3}$	$\frac{9}{2}\sqrt{\frac{1}{7}}$	3	7	4	$-\frac{45}{4}\sqrt{\frac{7}{143}}$	$\frac{315}{572}\sqrt{5}$
1	3	4	$-\frac{9}{4}$	$-\frac{9}{2}\sqrt{\frac{1}{7}}$	3	7	6	$\frac{39}{8}\sqrt{\frac{21}{374}}$	$\frac{819}{748}\sqrt{\frac{1}{5}}$
1	5	4	$-\frac{3}{2}\sqrt{3}$	$\frac{3}{2}\sqrt{\frac{15}{11}}$	3	7	8	$\frac{9}{8}\sqrt{\frac{7}{247}}$	$-\frac{189}{988}\sqrt{\frac{1}{5}}$
1	5	6	$-\frac{3}{2}\sqrt{\frac{5}{2}}$	$-\frac{3}{2}\sqrt{\frac{15}{11}}$	3	7	10	$-\frac{315}{8}\sqrt{\frac{3}{646}}$	$-\frac{945}{1292}\sqrt{5}$
3	3	0	$-\frac{3}{4}\sqrt{7}$	$\frac{3}{4}$	5	7	2	$-\frac{15}{2}\sqrt{\frac{1}{13}}$	$\frac{15}{26}\sqrt{\frac{21}{11}}$
3	3	2	$\frac{3}{8}\sqrt{21}$	$\frac{3}{4}$	5	7	4	$\frac{33}{4}\sqrt{\frac{15}{442}}$	$\frac{15}{442}\sqrt{231}$
3	3	4	$-\frac{3}{4}\sqrt{\frac{7}{22}}$	$\frac{9}{44}$	5	7	6	$-\frac{33}{4}\sqrt{\frac{5}{323}}$	$\frac{15}{646}\sqrt{231}$
3	3	6	$-\frac{15}{8}\sqrt{\frac{21}{11}}$	$-\frac{75}{44}$	5	7	8	$\frac{3}{4}\sqrt{\frac{105}{494}}$	$\frac{45}{494}\sqrt{\frac{21}{11}}$
3	5	2	$-\frac{3}{2}\sqrt{\frac{5}{2}}$	$\frac{5}{2}\sqrt{\frac{15}{77}}$	5	7	10	$\frac{99}{2}\sqrt{\frac{35}{193\,154}}$	$-\frac{3465}{193\,154}\sqrt{231}$
3	5	4	$\frac{11}{4}\sqrt{\frac{3}{13}}$	$\frac{3}{26}\sqrt{\frac{165}{7}}$	5	7	12	$-\frac{495}{4}\sqrt{\frac{7}{14\,858}}$	$-\frac{1485}{14\,858}\sqrt{231}$
3	5	6	0	0	7	7	0	$-\frac{3}{8}\sqrt{15}$	$\frac{3}{8}$
3	5	8	$-\frac{7}{2}\sqrt{\frac{15}{26}}$	$-\frac{7}{13}\sqrt{\frac{105}{11}}$	7	7	2	$\frac{795}{16}\sqrt{\frac{3}{3094}}$	$\frac{795}{1768}$
5	5	0	$-\frac{1}{2}\sqrt{11}$	$\frac{1}{2}$	7	7	4	$-\frac{5589}{16}\sqrt{\frac{5}{323\,323}}$	$\frac{150\,903}{369\,512}$
5	5	2	$\frac{3}{2}\sqrt{\frac{33}{26}}$	$\frac{15}{26}$	7	7	6	$\frac{375}{16}\sqrt{\frac{15}{7106}}$	$\frac{9375}{28\,424}$
5	5	4	$-\sqrt{\frac{22}{13}}$	$\frac{6}{13}$	7	7	8	$-\frac{375}{8}\sqrt{\frac{15}{79\,534}}$	$\frac{9375}{45\,448}$
5	5	6	$\sqrt{\frac{33}{85}}$	$\frac{4}{17}$	7	7	10	$\frac{243}{16}\sqrt{\frac{1}{193\,154}}$	$\frac{45\,927}{3863\,080}$
5	5	8	$7\sqrt{\frac{11}{2470}}$	$-\frac{49}{247}$	7	7	12	$\frac{1815}{16}\sqrt{\frac{3}{52\,003}}$	$-\frac{19\,965}{59\,432}$
5	5	10	$-\frac{105}{2}\sqrt{\frac{11}{4199}}$	$-\frac{6615}{4199}$	7	7	14	$-\frac{3003}{16}\sqrt{\frac{3}{14\,858}}$	$-\frac{429\,429}{297\,160}$

We will label $(\xi\eta\zeta)$ principal axes when atomic tensors $\langle T_r^K\rangle_{(\xi\eta\zeta)}$ for the model in question are zero unless $r = 0$. Alternatively, in principal axes, atomic tensors are said to be diagonal and the ζ-axis is called the axis of quantization.

It can be shown that the magnetic amplitude is zero if $\boldsymbol{k}$ is parallel to the axis of quantization, i.e. for $\boldsymbol{k}$ and $\boldsymbol{\zeta}$ parallel, $\langle \boldsymbol{Q}_\perp\rangle = 0$. This finding is a generalization of the standard result which says that the intensity is zero when $\boldsymbol{k}$ and the moment direction are parallel.

A second result of this nature is found for the value of $\boldsymbol{P}\cdot\langle\boldsymbol{Q}_\perp\rangle$ when $\boldsymbol{P}$ and $\boldsymbol{\zeta}$ are parallel. We find

$$\hat{\boldsymbol{\zeta}}\cdot\langle\boldsymbol{Q}_\perp\rangle = \sum_{K'}\left(\frac{3K'}{2K'+1}\right)^{1/2}\{\Psi_0^{K'}(K'-1)\}_{(\xi\eta\zeta)}[P_{K'-1}(k_\zeta) - P_{K'+1}(k_\zeta)], \tag{3.2}$$

where K' is odd, and $k_\zeta = \hat{\boldsymbol{k}}\cdot\hat{\boldsymbol{\zeta}}$ is the projection of the scattering wavevector on the axis of quantization. In arriving at (3.2), the term with $K = K'$ is found to vanish, and the two terms $K = K' \pm 1$ combine with the aid of (2.7) to give the very simple expression that we report. The Legendre polynomial $P_n(x)$ satisfies $P_0(x) = 1$ and $P_n(1) = 1$. From the second

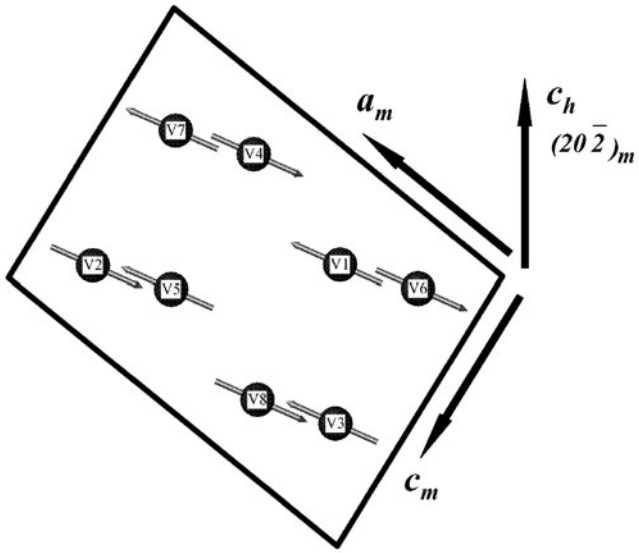

Figure 1. Positions of the eight V ions in the monoclinic cell adopted by V_2O_3 below the Néel temperature, together with the configuration of their moments in the plane spanned by $\boldsymbol{a}_m$ and $\boldsymbol{c}_m$. The monoclinic Bragg wavevector $\boldsymbol{\tau}_m = (20\bar{2})_m$ is parallel to the trigonal axis $\boldsymbol{c}_h$, and $\boldsymbol{b}_m$ is normal to the plane of the diagram and parallel to $\boldsymbol{a}_h$ [9].

property we see that scattering is zero if $\boldsymbol{k}$ and $\boldsymbol{\zeta}$ coincide, a result that we anticipated. For $K' = 1$ and 3,

$$1 - P_2(x) = \tfrac{3}{2}(1 - x^2) \qquad \text{and} \qquad P_2(x) - P_4(x) = \tfrac{7}{8}(1 - x^2)(5x^2 - 1). \tag{3.3}$$

4. Vanadium sesquioxide

The space group of the low-temperature monoclinic structure is number 15 ($I2/a$). This is a body-centred cell and Bragg wavevectors $\boldsymbol{\tau}_m(hkl)$ for charge reflections have the necessary condition $h+k+l$ an even integer (Miller indices h, k and l are integers). The antiferromagnetic configuration of vanadium magnetic moments, displayed in figure 1, consists of sheets of moments with ferromagnetic alignment within $(010)_m$ layers, or hexagonal (110) layers, and moment reversal between adjacent layers [12]. The moments are orientated along some easy axis in these layers, and we take ϕ as the canting angle with respect to the trigonal axis.

The trigonal basis vectors are $\boldsymbol{a}_h = a(1, 0, 0)$, $\boldsymbol{b}_h = a(-1/2, (1/2)\sqrt{3}, 0)$ and $\boldsymbol{c}_h = c(0, 0, 1)$ and the volume of the unit cell $= a^2c\sqrt{3}/2$. Following Dernier and Marezio [11] in the use of an I-centred cell, from these vectors we generate monoclinic basis vectors $\boldsymbol{a}_m = (0, \frac{1}{\sqrt{3}}2a, (1/3)c)$, $\boldsymbol{b}_m = \boldsymbol{a}_h$ and $\boldsymbol{c}_m = (0, \frac{1}{\sqrt{3}}a, -(1/3)c)$, and the volume of the cell $= a^2c/\sqrt{3}$. The corresponding Bragg wavevector $\boldsymbol{\tau}_m(hkl) \equiv (hkl)_m$ is

$$\boldsymbol{\tau}_m(hkl) = \frac{1}{a}\left(k, \frac{1}{\sqrt{3}}(h + l), \frac{a}{c}(h - 2l)\right). \tag{4.1}$$

We note that $(l0\bar{l})_m$ is parallel to $\boldsymbol{c}_h$ and $(2lkl)_m$ is normal to $\boldsymbol{c}_h$.

Referring to figure 1, the position coordinates of vanadium ions labelled (1) and (5) are (x, y, z) and $(-x, -y, -z)$, respectively, with $x = 0.3439$, $y = 0.0012$ and $z = 0.2993$ [11]. The positions of the pair (2) and (6) are related by a body-centre translation to the pair (1) and (5).

The position coordinates of (3) and (7) are $(1/2-x, y, -z)$ and $(1/2+x, -y, z)$, respectively, and the pairs (4), (8) and (3), (7) are related by the body-centre translation. The body-centre translation $(1/2, 1/2, 1/2)_m = \frac{a}{2}(1, \sqrt{3}, 0)$ and $(1/2, 1/2, 1/2)_m \cdot \boldsymbol{\tau}_m(hkl) = \frac{1}{2}(h+k+l)$. It is convenient to define an angle $\nu = 2\pi(x, y, z)_m \cdot \boldsymbol{\tau}_m(hkl) = 2\pi(xh + zl)$ where the second equality is correct for $y = 0$.

For the model of V_2O_3 that we have described, in the previous paragraphs, $\Psi^{K'}$ can be different from zero for even values of $K'+(h+k+l)$, so there is a selection rule in the structure factor that links the rank of atomic tensors and the sum of Miller indices [9]. Neutron magnetic diffraction is observed at reflections with $h + k + l$ an odd integer, i.e. space-group-forbidden reflections, and the scattering amplitude is composed of tensors of rank $K' = 1$, 3 and 5. One finds

$$\Psi^{K'}_{q'}(K) = 4\cos(\nu)\{\langle T^{K'}_{q'}(K)\rangle + (-1)^h \langle T^{K'}_{-q'}(K)\rangle\}. \tag{4.2}$$

Moon [12] studied reflections with even h and established the configuration of moments illustrated in figure 1, in which V moments are contained in the plane normal to $\boldsymbol{b}_m$ and cant at angle $\phi \sim 70^\circ$ with respect to $\boldsymbol{c}_h$. Intensity observed with odd h using resonant x-ray diffraction [6] has been successfully interpreted using (4.2) [9]. Note that for odd h we have $\Psi^{K'}_{q'} = -\Psi^{K'}_{-q'}$ and there is no contribution to scattering from diagonal elements of the atomic tensor. Scattering observed at space-group-forbidden reflections with odd h is the magnetic analogue of Templeton and Templeton x-ray scattering [13] by anisotropic charge distributions.

4.1. Magnetic reflections with even h

The atomic tensor in (4.2) is obtained from principal axes $(\xi\eta\zeta)$ using (3.1). It is assumed that the axis of quantization is contained in the plane $\boldsymbol{a}_m$–$\boldsymbol{c}_m$ and it encloses an angle ϕ with the trigonal axis. One finds

$$\langle T^{K'}_{q'}(K)\rangle = \langle T^{K'}_{0}(K)\rangle_{(\xi\eta\zeta)} D^{K'}_{q'0}\left(-\frac{\pi}{2}, \phi, 0\right), \tag{4.3}$$

and the corresponding value of the structure factor is

$$\Psi^{K'}_{q'}(K) = 8\cos(\nu)\langle T^{K'}_{0}(K)\rangle_{(\xi\eta\zeta)} D^{K'}_{q'0}\left(-\frac{\pi}{2}, \phi, 0\right). \tag{4.4}$$

The last result follows because, according to (4.3), $\langle T^{K'}_{q'}\rangle = \langle T^{K'}_{-q'}\rangle$. (In consequence, for odd h the result (4.3) predicts null scattering.)

Using (4.4) in (2.8) we arrive at

$$I_{\text{crystal}} = \{8\cos(\nu)\}^2 \sum_{K'I'}\sum_{l}(2l+1)^{1/2} G(K', I'; l) P_l(\tau_\zeta)\langle T^{K'}_0(K'-1)\rangle_{(\xi\eta\zeta)} \times \langle T^{I'}_0(I'-1)\rangle_{(\xi\eta\zeta)} \begin{pmatrix} K' & I' & l \\ 0 & 0 & 0 \end{pmatrix}. \tag{4.5}$$

On writing $\hat{\boldsymbol{\tau}}_m(hkl) = (t_1, t_2, t_3)$ one has $\tau_\zeta = t_2 \sin\phi + t_3 \cos\phi$. If $\hat{\boldsymbol{\tau}}_m$ and $\boldsymbol{\zeta}$ are parallel, $\tau_\zeta = 1$ and the intensity is zero by virtue of the sum rule (2.9) which is satisfied by $G(K', I'; l)$. On retaining in (4.5) the term $K' = I' = 1$, and neglecting all other terms in the sums on K' and I', the remaining $l = 0$ and 2 terms collapse to give

$$I_{\text{crystal}} = \tfrac{9}{4}\{8\cos(\nu)\}^2(1-\tau_\zeta^2)\langle T^1_0(0)\rangle^2_{(\xi\eta\zeta)}. \tag{4.6}$$

In arriving at this expression we use entries in table 1 and for the Legendre polynomials the first entry in (3.3). The result (4.6) is consistent with the more general expression found in (2.11).

The intensity (4.5) contains the canting angle ϕ and three atomic tensors. These four unknown quantities can be inferred by fitting experimental data for intensities to (4.5). Values

Table 2. Matrix elements $\langle T_0^{K'}(K'-1)\rangle = \langle SM_S LM_L|T_0^{K'}(K'-1)|SM_S LM_L\rangle$ with $S = 1$, $M_S = 1$, $L = 3$ and $M_L = -3$ and 1 that enter the evaluation of the intensity when the V-ion wavefunction in V_2O_3 is modelled by (4.7).

$M_L = -3$	$M_L = 1$
$\langle T_0^1(0)\rangle = -\frac{1}{5}\langle j_0(k)\rangle - \frac{22}{21}\langle j_2(k)\rangle$	$\langle T_0^1(0)\rangle = \langle j_0(k)\rangle + \frac{38}{105}\langle j_2(k)\rangle$
$\langle T_0^3(2)\rangle = \frac{4}{7\sqrt{7}}\{\langle j_2(k)\rangle + \langle j_4(k)\rangle\}$	$\langle T_0^3(2)\rangle = \frac{4}{7\sqrt{7}}\{\frac{1}{5}\langle j_2(k)\rangle + \frac{2}{3}\langle j_4(k)\rangle\}$
$\langle T_0^5(4)\rangle = -\frac{1}{7}(\frac{15}{11})^{1/2}\langle j_4(k)\rangle$	$\langle T_0^5(4)\rangle = -\frac{1}{7}(\frac{5}{33})^{1/2}\langle j_4(k)\rangle$

of the atomic tensors derived from a model of the V ion's wavefunction can then be tested against measured values.

We have calculated (4.5) using for $\langle T_0^{K'}(K'-1)\rangle_{(\xi\eta\zeta)}$ expressions derived from a model V wavefunction based on $3d^2$ and the configuration ^3F, namely,

$$|G\rangle = |S = 1, M_s = 1\rangle\{\varepsilon|L = 3, M_L = -3\rangle + (1-\varepsilon^2)^{1/2}|L = 3, M_L = 1\rangle\}. \tag{4.7}$$

The value $\varepsilon = 0.671$ gives $\langle L_\zeta\rangle = -0.8$ and a V magnetic moment $\mu = 1.2\ \mu_B$ in agreement with the finding of Moon [12]. In the expression for $\langle T_0^{K'}(K'-1)\rangle_{(\xi\eta\zeta)}$ there are no contributions from cross-terms and one finds

$$\begin{aligned}\langle T_0^{K'}(K'-1)\rangle_{(\xi\eta\zeta)} &= \varepsilon^2\langle SM_s = 1, LM_L = -3|T_0^{K'}(K'-1)|SM_s = 1, LM_L = -3\rangle \\ &\quad + (1-\varepsilon^2)\langle SM_s = 1, LM_L = 1|T_0^{K'}(K'-1)|SM_s = 1, LM_L = 1\rangle. \end{aligned}\tag{4.8}$$

Expressions for the two matrix elements, obtained by use of (A.8), are listed in table 2. In our numerical estimates we use $\langle j_n(k)\rangle$ for V^{3+} from [14].

Regarding $\langle T_0^1(0)\rangle_{(\xi\eta\zeta)}$ that appears in the approximation (4.6) to I_{crystal}, our model wavefunction gives

$$\langle T_0^1(0)\rangle_{(\xi\eta\zeta)} = \tfrac{1}{3}\langle j_0(k)\rangle(3-4\varepsilon^2) + \tfrac{2}{105}\langle j_2(k)\rangle(19-74\varepsilon^2). \tag{4.9}$$

As anticipated in (2.5), the coefficient of $\langle j_0\rangle/3$ is the magnetic moment μ of the V ion.

A confrontation of experimental data for magnetic Bragg intensities with I_{crystal} listed in the second ($\varepsilon^2 = 0.45$, $\langle L_\zeta\rangle = -0.8$) and third ($\varepsilon^2 = 0.25$, $\langle L_\zeta\rangle = 0$) columns of table 3 will help find the exact nature of the magnetization and settle the contribution to it made by the orbital moment. The value of the canting angle $\phi = 70^\circ$ is consistent with the interpretation of neutron and resonant x-ray diffraction data [9, 12].

Matching reflections, identified by a common value of $|\tau_m|$, are particularly valuable because uncertainty in the interpretation arising from uncertainty in $\langle j_n(k)\rangle$ is eliminated. To a good approximation, $(210)_m$&$(2\bar{1}0)_m$ and $(201)_m$ are a group of matching reflections and the difference between I_{crystal} at the partners $(210)_m$&$(2\bar{1}0)_m$ and $(201)_m$ is striking and is largely due to pronounced anisotropy in the magnetization. Two other groups of matching reflections that are very sensitive to anisotropy are $(003)_m$&$(40\bar{1})_m$ and $(023)_m$&$(02\bar{3})_m$, $(42\bar{1})_m$&$(4\bar{2}\bar{1})_m$. These two groups of reflections are sensitive to the orbital magnetization, which is seen in the variation of the ratio in column five between I_{crystal} for $\langle L_\zeta\rangle = -0.8$ and that for $\langle L_\zeta\rangle = 0$. In this respect, we note that the last three reflections in table 3 have intensity due to the orbital magnetization and so they appear to be particularly good sources of information.

4.2. Magnetic reflections with odd h

We have estimated the neutron scattering intensity at magnetic reflections with h odd by using atomic tensors inferred from a successful interpretation of resonant x-ray diffraction

Table 3. The second column contains $I_{\rm crystal}$ derived from (4.5) and atomic tensors (4.8) evaluated for $\varepsilon^2 = 0.45$ which gives a V-ion moment $\mu = 1.2\ \mu_B$. Values are listed with increasing magnitudes of selected Bragg wavevectors $\boldsymbol{\tau}_m = (hkl)_m$, and the last three columns specify the unit vector $\hat{\tau}_m = (t_1, t_2, t_3)$. The third column contains $I_{\rm crystal}$ derived from (4.5) and (4.8) and $\varepsilon^2 = 0.25$ which corresponds to a V-ion moment with no orbital content $\langle L_\zeta \rangle = 0$ and $\mu = 2.0\ \mu_B$. The ratio of $I_{\rm crystal}$ for $\mu = 1.2$ and $2.0\ \mu_B$, normalized to unity at the strongest reflection $(010)_m$, is found in the fifth column. The canting angle $\phi = 70°$.

h	k	l	$\langle L \rangle = -0.8$	$\langle L \rangle = 0.0$	$\lvert\boldsymbol{\tau}\rvert$ (Å^{-1})	Ratio	t_1	t_2	t_3
0	1	0	16.61	50.12	0.20	1.00	1.000	0.000	0.000
0	0	1	1.47	4.33	0.18	1.02	0.000	0.643	−0.766
2	0	−1	3.94	12.36	0.30	0.96	0.000	0.387	0.922
2	1	0	0.62	1.95	0.34	0.96	0.597	0.689	0.410
2	0	1	1.34	4.08	0.35	0.99	0.000	1.000	0.000
0	1	2	3.59	14.46	0.41	0.75	0.487	0.562	−0.669
0	2	1	0.42	1.88	0.44	0.68	0.912	0.263	−0.314
2	1	−2	2.76	12.41	0.46	0.67	0.436	0.000	0.900
2	2	−1	1.63	7.77	0.50	0.63	0.802	0.231	0.551
2	2	1	2.09	9.17	0.53	0.69	0.756	0.655	0.000
0	0	3	1.26	7.12	0.54	0.53	0.000	0.643	−0.766
4	0	−1	0.87	3.15	0.54	0.83	0.000	0.643	0.766
4	1	0	0.30	1.07	0.57	0.84	0.349	0.805	0.479
0	3	0	0.84	7.99	0.60	0.32	1.000	0.000	0.000
2	0	3	0.67	3.32	0.64	0.61	0.000	0.903	−0.430
0	2	3	0.23	3.14	0.67	0.22	0.596	0.516	−0.615
4	2	−1	0.57	3.03	0.67	0.56	0.596	0.516	0.615
4	0	−3	0.43	3.94	0.70	0.33	0.000	0.166	0.986
4	1	2	0.28	1.21	0.72	0.71	0.277	0.961	0.000
2	2	3	0.22	1.98	0.75	0.34	0.530	0.765	−0.365
2	3	−4	0.21	0.35	0.94	1.81	0.637	−0.245	0.730
0	5	0	0.32	0.15	1.00	6.45	1.000	0.000	0.000
0	5	2	0.24	0.03	1.06	21.44	0.941	0.217	−0.259
2	5	−2	0.27	0.02	1.08	33.00	0.924	0.000	0.381
0	4	5	0.30	0.00	1.20	612.25	0.665	0.480	−0.572
2	5	−4	0.52	0.01	1.24	107.54	0.810	−0.187	0.556
4	4	−5	0.22	0.00	1.26	153.71	0.637	−0.092	0.766

on magnetically ordered V_2O_3. The intensity of scattering from a single crystal is derived from (2.8). For the reflections of interest here, the nuclear structure factor is zero, and thus polarization in the primary beam of neutrons does not lead to mixed magnetic and nuclear reflections. Because the V magnetic moment is contained in the plane spanned by $\boldsymbol{a}_m$ and $\boldsymbol{c}_m$, $\Psi^1_{\pm 1} = 0$. Our estimate of $I_{\rm crystal}$ is made with tensors of rank $K' = 3$ and the terms proportional to $\langle j_2(k) \rangle$. Terms we neglect are proportional to $\langle j_4(k) \rangle$, cf table 2, which for $k \sim 0.6$ Å^{-1} is very small compared to $\langle j_2(k) \rangle$ that we retain.

By way of orientation, first we consider the intensity (2.6) observed in a powder pattern. Setting $K' = 3$ and using (2.7),

$$I_{\rm powder} = \tfrac{3}{4} \sum_{q'} |\Psi^3_{q'}(2)|^2.$$

In the sum, q' takes all values consistent with the rank $K' = 3$ of the tensor, but for odd h, $\Psi^{K'}_0 = 0$. Since the V ion occupies a site with no symmetry, site symmetry plays no part in selecting values of the projection label q' on atomic tensors.

Table 4. Values of atomic tensors of rank three for V ions in magnetically ordered V_2O_3 inferred from an interpretation of resonant x-ray Bragg diffraction [15].

$\langle T^3_{+1}(2)\rangle' = (0.037 \pm 0.009)\langle j_2(k)\rangle$
$\langle T^3_{+2}(2)\rangle'' = (-0.017 \pm 0.014)\langle j_2(k)\rangle$
$\langle T^3_{+3}(2)\rangle' = (0.039 \pm 0.013)\langle j_2(k)\rangle$

Table 5. Estimates for V_2O_3 of the single-crystal intensity (2.8) and projections of the magnetic amplitude on $\boldsymbol{c}_h$ and $\boldsymbol{b}_m$.

Reflection	$I_{\rm crystal}$	$\boldsymbol{c}_h \cdot \langle \boldsymbol{Q}_\perp \rangle$	$\hat{\boldsymbol{b}}_m \cdot \langle \boldsymbol{Q}_\perp \rangle$
$(102)_m$	0.007	0	0.084
$(120)_m$	0.002	0.027	0.004
$(122)_m$	0.011	0.063	−0.036
$(320)_m$	0.022	−0.118	−0.016
$(140)_m$	0.001	0.021	0.002
$(340)_m$	0.017	−0.091	−0.016

In (4.2) we set h odd and use $\langle T^{K'}_{-q'}\rangle = (-1)^{q'}\langle T^{K'}_{q'}\rangle^*$ and find

$$\Psi^3_{+1}(2) = 8\cos(\nu)\langle T^3_{+1}(2)\rangle',$$
$$\Psi^3_{+2}(2) = \mathrm{i}\,8\cos(\nu)\langle T^3_{+2}(2)\rangle'',$$
$$\Psi^3_{+3}(2) = 8\cos(\nu)\langle T^3_{+3}(2)\rangle'.$$

Values of the atomic tensors inferred from an interpretation of resonant x-ray diffraction data on V_2O_3 [6, 15] are listed in table 4. Our knowledge of $\langle T^3_{+2}\rangle''$ is not as good as that for $\langle T^3_{+1}\rangle'$ and $\langle T^3_{+3}\rangle'$. From entries in table 4 we find

$$I_{\rm powder} = 96\cos^2(\nu)\{\langle T^3_{+1}(2)\rangle'^2 + \langle T^3_{+2}(2)\rangle''^2 + \langle T^3_{+3}(2)\rangle'^2\} \sim 0.31\{\langle j_2(k)\rangle\cos(\nu)\}^2.$$

Let us consider the reflection $(340)_m$ for which $\tau(340)_m = 0.90$ Å^{-1} and $\cos(\nu) = 0.98$. Using [14] $\langle j_2(\tau)\rangle = 0.20$, we obtain for $(340)_m$ the estimate $I_{\rm powder} \sim 0.011$. Table 5 contains estimates of intensities for single crystals derived from (2.8). Reflections $(122)_m$ and $(320)_m$ possess the same value of τ_m, as is evident by inspection of (4.1).

Spatial anisotropy in the intensities is highlighted in projections of $\langle \boldsymbol{Q}_\perp\rangle$. Accordingly, table 5 contains some values of $\boldsymbol{m}\cdot\langle \boldsymbol{Q}_\perp\rangle$ for $\boldsymbol{m}$ parallel to the trigonal axis $\boldsymbol{c}_h$ and $\boldsymbol{m}$ normal to the plane $\boldsymbol{a}_m$–$\boldsymbol{c}_m$ that contains the V magnetic moments. The amplitude $\hat{\boldsymbol{c}}_h \cdot \langle \boldsymbol{Q}_\perp\rangle$ is proportional to t_1 and vanishes for reflections $(h0l)$. In detail,

$$\hat{\boldsymbol{c}}_h \cdot \langle \boldsymbol{Q}_\perp\rangle = \sqrt{21}t_1\cos(\nu)\{\langle T^3_{+1}\rangle' t_3(15t_3^2 - 11) + 2\sqrt{10}\langle T^3_{+2}\rangle'' t_2(1 - 3t_3^2) + \sqrt{15}\langle T^3_{+3}\rangle' t_3(t_1^2 - 3t_2^2)\}. \quad (4.10)$$

Expressions for other projections are even more complicated and we refrain from giving them.

5. Discussion

In the context of an atomic model of a material, we have developed and applied a theoretical framework for magnetic neutron diffraction. The framework has the same formal structure as one used recently for the successful interpretation of resonant x-ray Bragg diffraction by magnetic crystals. A formal structure in the interpretation of diffraction data that is common to neutron and x-ray techniques facilities the comparison of results. By way of illustrating this advantage, we predict results for magnetic neutron diffraction by V_2O_3 on the basis of results

from resonant x-ray diffraction by the material that reveal reflections not yet observed with the neutron technique.

A new expression that we give for the intensity of neutrons magnetically diffracted by a single crystal is well suited to the identification of features due to spatial anisotropy in the distribution of magnetization. In this expression, the leading term is the intensity expected from a powder sample. Other general results include properties of the amplitude for magnetic diffraction when set in principal axes, where atomic spherical tensors describing the valence shell are diagonal. The atomic tensors have been expressed in terms of unit tensors that are widely used in atomic physics. The literature on the interpretation of x-ray dichroic signals and resonant diffraction already contains extensive tabulations of the unit tensors evaluated for 3d transition and lanthanide ions, and the results complement tabulations of closely related quantities that have been used in the interpretation of magnetic neutron diffraction signals.

Acknowledgments

We are grateful to Kevin S Knight for several valuable discussions and the creation of the figure, and to Devinder S Sivia for calculating entries in table 4. Our presentation has benefited from comments given by Jane Brown, who also spotted an inconsistency in our original calculation of entries in table 3. One of us (EB) is grateful to the director of the ISIS Facility, RAL, for hospitality during the course of the work.

Appendix

The purpose of the appendix is to record key expressions for the atomic tensor and to relate work to previous findings. The reduced matrix element in the Wigner–Eckart theorem,

$$\langle JM|T^{K'}_{q'}(K)|J'M'\rangle = (-1)^{J-M}\begin{pmatrix} J & K' & J' \\ -M & q' & M' \end{pmatrix}(SLJ\|T^{K'}(K)\|S'L'J'), \tag{A.1}$$

is simply related to quantities $A(K, K')$ and $B(K, K')$ used previously [7, 8] in the spin and orbital matrix elements of $T^{K'}$, namely,

$$(SLJ\|T^{K'}(K)\|S'L'J') = (-1)^{K'+J'-J}(2J+1)^{1/2}\{A(K, K') + B(K, K')\}. \tag{A.2}$$

We will not review properties of $A(K, K')$ and $B(K, K')$ but refer the reader to [7, 8] for this information. Tables of $A(K, K')$ and $B(K, K')$ for various ions are found in [8].

Let us, however, express the spin and orbital contributions to the reduced matrix element in terms of a standard reduced matrix element in atomic physics $W^{(ab)K'}$ used also in the interpretation of resonant x-ray diffraction. In $W^{(ab)K'}$ the integer a is the rank of its spin contribution, and b is the rank of its orbital contribution. Tables of $W^{(ab)K'}$, and $W^{(ab)}$ used in (A.8), are found in [10].

Writing

$$(SLJ\|T^{K'}(K)\|S'L'J') = Z^{K'}_{\text{spin}}(K) + Z^{K'}_{\text{orb}}(K), \tag{A.3}$$

we find

$$\begin{aligned} Z^{K'}_{\text{orb}}(K'-1) = {} & (-1)^{K'}\mathrm{i}^{K'+1}\delta_{S,S'}\{\langle j_{K'-1}(k)\rangle + \langle j_{K'+1}(k)\rangle\} \\ & \times [\tfrac{2}{3}(K'+1)]^{1/2}(2l+1)^2 A(K', K', l)W^{(0K')K'}, \end{aligned} \tag{A.4}$$

where K' is an odd integer, l is the angular momentum of the valence shell ($l = 2$ and 3, respectively, for 3d and lanthanide ions) and $A(K', K', l)$ is given in [7, 8]. $Z^{K'}_{\text{orb}}(K' \pm 1)$

satisfies (2.7) and $Z^{K'}_{\rm orb}(K')$ is zero. The spin contribution in (A.3) is slightly more complicated. Let us use

$$D(K,K') = (-1)^l \langle j_K(k)\rangle (2l+1) \begin{pmatrix} l & K & l \\ 0 & 0 & 0 \end{pmatrix} [\tfrac{3}{2}(2K+1)]^{1/2} W^{(1K)K'}. \tag{A.5}$$

If K' is even, the only non-zero value of $B(K,K')$ occurs when $K = K'$, in which case

$$Z^{K'}_{\rm spin}(K') = {\rm i}^{K'} [\tfrac{1}{3}(2K'+1)]^{1/2} D(K',K'). \tag{A.6}$$

If K' is odd, then $K = K' \pm 1$ and $Z^{K'}_{\rm spin}(K' \pm 1)$ satisfies (2.7). For $K = K' - 1$,

$$Z^{K'}_{\rm spin}(K'-1) = {\rm i}^{K'-1}[3(2K'+1)]^{-1/2}\{(K'+1)D(K'-1,K') - [K'(K'+1)]^{1/2} D(K'+1,K')\}. \tag{A.7}$$

The form of the Wigner–Eckart theorem quoted in (A.1) is appropriate when working with states labelled by the total angular momentum J. In describing properties of a 3d transition ion it is quite common to have states labelled by spin and orbital quantum numbers, $SM_S LM_L$, with

$$|SM_S LM_L\rangle = \sum_{JM} (SM_S LM_L | JM) |JM\rangle.$$

By constructing a matrix element $\langle SM_S LM_L | T^{K'}_{q'} | SM'_S LM'_L\rangle$ and performing sums on JM and $J'M'$, one finds that the appropriate form of the Wigner–Eckart theorem is obtained by replacing the quantity

$$(-1)^{J-M} \begin{pmatrix} J & K' & J' \\ -M & q' & M' \end{pmatrix} W^{(ab)K'}$$

by the expression

$$(-1)^{a+b+q'} \left\{ \frac{2K'+1}{(2a+1)(2b+1)} \right\}^{1/2} W^{(ab)} \sum_{mn} \begin{pmatrix} a & K' & b \\ -m & q' & -n \end{pmatrix} \times (-1)^{S-M_S} \begin{pmatrix} S & a & S' \\ -M_S & m & M'_S \end{pmatrix} (-1)^{L-M_L} \begin{pmatrix} L & b & L' \\ -M_L & n & M'_L \end{pmatrix}. \tag{A.8}$$

The reduced matrix elements $W^{(ab)}$ and $W^{(ab)K'}$ are related by a $9j$ symbol, and the general expression is

$$W^{(ab)K'} = \left\{ \frac{(2J+1)(2K'+1)(2J'+1)}{(2a+1)(2b+1)} \right\}^{1/2} \begin{Bmatrix} S & S' & a \\ L & L' & b \\ J & J' & K' \end{Bmatrix} W^{(ab)}. \tag{A.9}$$

Properties of $W^{(ab)}$ that are relevant to the interpretation of neutron diffraction are discussed in [16].

The contribution to Thomson scattering made by valence electrons is

$$\left\langle \sum_j \exp({\rm i}\boldsymbol{k}\cdot\boldsymbol{R}_j) \right\rangle = (4\pi)^{1/2} \sum_{Kq} \langle j_K\rangle Y^K_q(\hat{\boldsymbol{k}})^* \langle T^K_q\rangle_c. \tag{A.10}$$

Scattering by valence electrons will describe charge intensity seen at space-group-forbidden reflections, for which the unit-cell structure factor (2.3) satisfies $\Psi^K_{q=0} = 0$. In this instance, the Thomson structure factor is obtained from (A.10) by substituting Ψ^K_q for $\langle T^K_q\rangle_c$. The reduced matrix element of the charge atomic tensor is

$$(SLJ\|T^K\|S'L'J')_c = {\rm i}^K \sqrt{8\pi}\,(l\|Y^K\|l) W^{(0K)K}. \tag{A.11}$$

The reduced matrix element of a spherical harmonic in (A.11) limits K to even integers and a maximum $K = 2l$ (at space-group-forbidden reflections, the minimum $K = 2$).

References

[1] Brown P J 1993 *Int. J. Mod. Phys.* B **7** 3029
[2] Tokura Y and Nagaosa N 2000 *Science* **288** 462
[3] O'Handley R C 2000 *Modern Magnetic Materials* (New York: Wiley)
[4] Trammell G T 1953 *Phys. Rev.* **92** 1387
[5] Finkelstein K D *et al* 1992 *Phys. Rev. Lett.* **69** 1612
[6] Paolasini L *et al* 1999 *Phys. Rev. Lett.* **82** 4719
Paolasini L *et al* 2001 *J. Electron. Spectrosc. Relat. Phenom.* **120** 1
[7] Lovesey S W 1987 *Theory of Neutron Scattering from Condensed Matter* vol 2 (Oxford: Clarendon)
[8] Balcar E and Lovesey S W 1989 *Theory of Magnetic Neutron and Photon Scattering* (Oxford: Clarendon)
Osborn R *et al* 1991 *Handbook on the Physics and Chemistry of Rare Earths* vol 14 (Amsterdam: North-Holland)
[9] Lovesey S W *et al* 2002 *Phys. Rev.* B **65** 224402
[10] Lovesey S W and Balcar E 1997 *J. Phys.: Condens. Matter* **9** 4237
[11] Dernier P D and Marezio M 1970 *Phys. Rev.* B **2** 3771
[12] Moon R M 1970 *Phys. Rev. Lett.* **25** 527
[13] Templeton D H and Templeton L K 1994 *Phys. Rev.* B **49** 14850
[14] Brown P J 1995 *International Tables for Crystallography* vol C (Dordrecht: Kluwer Academic)
[15] Lovesey S W *et al* 2001 *2nd Int. Workshop on Electron Correlations and Materials Properties* ed A Gonis and N Kioussis (New York: Kluwer Academic)
[16] Balcar E and Lovesey S W 1988 *J. Phys. C: Solid State Phys.* **21** L1127